Petroleum 2 (2016) 148–155

Contents lists available at ScienceDirect

Petroleum

journal homepage: www.keaipublishing.com/en/journals/petlm

Unconventional resource's production under desorption-induced effects

S. Sina Hosseini Boosari [a], Umut Aybar [b], Mohammad O. Eshkalak [b, *]

[a] Petroleum and Natural Gas Engineering, Department at West Virginia University, USA
[b] Petroleum and Geosystems Engineering, Department at the University of Texas at Austin, USA

ARTICLE INFO

Article history:
Received 15 November 2015
Received in revised form
5 February 2016
Accepted 21 February 2016

Keywords:
Shale desorption
Unconventional reservoirs
Porosity change
Permeability change
Desorption-induced effect

ABSTRACT

Thousands of horizontal wells are drilled into the shale formations across the U.S. and hydrocarbon production is substantially increased during past years. This fact is accredited to advances obtained in hydraulic fracturing and pad drilling technologies. The contribution of shale rock surface desorption to production is widely accepted and confirmed by laboratory and field evidences. Nevertheless, the subsequent changes in porosity and permeability due to desorption combined with hydraulic fracture closures caused by increased net effective rock stress state, have not been captured in current shale modeling and simulation. Hence, it is essential to investigate the effects of induced permeability, porosity, and stress by desorption on ultimate hydrocarbon recovery.

We have developed a numerical model to study the effect of changes in porosity, permeability and compaction on four major U.S. shale formations considering their Langmuir isotherm desorption behavior. These resources include; Marcellus, New Albany, Barnett and Haynesville Shales. First, we introduced a model that is a physical transport of single-phase gas flow in shale porous rock. Later, the governing equations are implemented into a one-dimensional numerical model and solved using a fully implicit solution method. It is found that the natural gas production is substantially affected by desorption-induced porosity/permeability changes and geomechancis. This paper provides valuable insights into accurate modeling of unconventional reservoirs that is more significant when an even small correction to the future production prediction can enormously contribute to the U.S. economy.

1. Introduction

Recoverable reserves of shale gas in the U.S. are estimated to be 862 Tcf [1]. Although challenges associated to exploration and management of shale assets are yet to be resolved, decreased evaluated risk promises a secure gas supply for next decades. The large accumulation of gas shale formations serve as both a hydrocarbon source and a productive reservoir. Most of the gas is stored in organic-rich rock while less portion of gas in place is in pore spaces [2]. Extremely low matrix permeability as well as highly complex network of natural fractures are unique characteristics of shale formations. Permeability of shale rocks is estimated to be between 50 nD (nano-Darcy) and 150 nD [3]. Recent advances and innovations in hydraulic fracturing are key success of shale gas economic production as a viable global energy supply. Nevertheless, complexities associated with flow mechanisms and existence of many pressure dependent phenomena, such as combined hydraulic and natural fracture conductivity losses, Klinkenberg gas slippage effect, desorption/adsorption and Darcy/non-Darcy flow, are not completely understood and need more attentions to reach our industry needs. In this study, desorption-induced porosity and permeability changes of shale matrix as well as closure effect of hydraulic fractures are focused in detail to evaluate their impact on production form four very productive U.S. shale resources.

* Corresponding author. Tel.: +1 512 919 0844.
E-mail address: eshkalak@utexas.edu (M.O. Eshkalak).
Peer review under responsibility of Southwest Petroleum University.

Production and Hosting by Elsevier on behalf of KeAi

http://dx.doi.org/10.1016/j.petlm.2016.02.004

Hydraulic fracturing creates highly conductive channels and paths for the reservoir fluid to flow from the reservoir pay zone to the well bore. Moreover, stress-induced natural fractures open with the hydraulic fracturing operation; thus a secondary fracture network is created in addition to hydraulic fractures. This secondary fracture network placed in the stimulated reservoir volume (SRV) area is caused by stress alterations during hydraulic fracturing treatment [4]. Researchers named this secondary fracture network either as natural fractures or secondary fracture network [5]. The main difference between primary fractures, which are hydraulic fractures, and secondary fractures is that the secondary fracture network is unpropped. Typical proppant volumes used in the hydraulic fracture operations are very low to keep fractures open in the propped secondary fracture network. Therefore, these secondary fractures remain unpropped (Since the natural fractures lack proppant, their conductivities are much more pressure dependent compared to hydraulic fractures.). Pressure-dependency of hydraulic fractures and their impact on production are discussed by the researchers [2,6,7] and are combined with desorption-induced porosity/permeability change in this study.

Reservoir simulation and modeling of unconventional resources have been given much more attention over the past years. Many numerical and analytical models are developed and extensive reservoir studies have been conducted. Commercial reservoir simulators are also improved to handle and capture fluid flow behavior and natural gas production from unconventional assets, such as shale. However, the developed models have ignored some of complex physics of shale and integrating the entire phenomena in shale is still a challenging target for the petroleum industry. Further, among analytical and semi-analytical methods, works done by Refs. [8–11] have provided comprehensive progress in the modeling of shale gas reservoirs.

Porosity, permeability and gas desorption of shale are considered the key parameters that affect shale ultimate gas recovery. However, least amount of simulation studies is conducted to account for porosity and permeability change due to desorption and rock compaction. In this paper, we first derived the porosity changes due to compaction and desorption, second, we plot the porosity and permeability versus the pressure for Marcellus, Barnett, New Albany and Haynesville shale. Afterward, we introduce a physical model of a horizontal well and the appropriate nonlinear partial differential equations created from governing equations are solved numerically through fully implicit method. The gas production from a single pair of hydraulic fractures is then scaled up to the entire horizontal well for each specific reservoir.

2. Shale desorption isotherms

Large portion of shale rock consists of organic matter, kerogenic media. Natural gas methane molecules are adsorbed on the organic rich strata (also they are stored in pore spaces and natural fractures). Thus, significant amount of natural gas can be produced from the surface of kerogen, which is also known as total organic carbon, TOC [12]. By its very nature, in order to release methane stored within the shale, it is necessary to enhance fluid pathways (create fractures) and deplete the surrounding pressure. As the pressure decreases due to production, more and more adsorbed gas is released from the surface of matrix; this contributes to the total amount of gas produced. Therefore, an adsorption model is required to predict the gas desorbed from shale matrix that will also be served to determine the first objective of this study, calculating the desorption-induced porosity/permeability.

Langmuir adsorption model [13] is the most common empirical mathematical model used to quantify the amount of desorbed gas as a function of pore pressure at constant temperature. This analogy comes from the developments made in modeling coal bed methane (pre-shale technology), but it must be noted that sorptive characteristics of shale might not necessarily serve the same way as it does in shale [14].

Langmuir model simply represents a nonlinear relationship between the potential amount of releasable-gas and the pore pressure given by Eq. (1). This equation represents that the potential amount of releasable-gas is only a function of reservoir pressure.

$$G = \frac{V_L P}{P + P_L} \tag{1}$$

where G is the potential releasable-gas content in scf/t, P is reservoir pressure (assumed to be the average reservoir pressure) in psi, and V_L (Langmuir volume) in scf/t and P_L (Langmuir pressure) in psi are Langmuir constants. Laboratory tests are necessary to determine V_L and P_L from core samples. Langmuir pressure is defined as the pressure at which 50% of gas is desorbed. By this definition, it is clear that the higher the Langmuir pressure reaches, more released-gas from the organic shale matter. Langmuir volume is the gas volume at infinite pressure representing the maximum storage capacity of gas, which is a function of TOC of the particular shale sample.

Fig. 1 shows the capability of four U.S. shale formations in releasing gas that is characterized through Langmuir model. These assets are, Marcellus, New Albany, Barnett and Haynesville shale.

Table 1 provides the common values of properties used in this study for the aforementioned assets. All of them are gathered from the numerical modeling literature except the critical pressure that is calculated using Eq. (2), that is also explained in detail in the subsequent section.

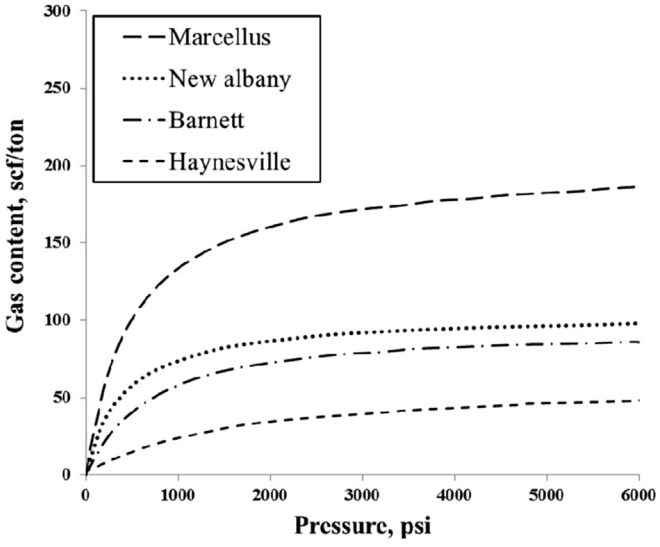

Fig. 1. Desorption isotherms for four U.S. shale formations.

Table 1
General properties of four U.S. shale formations.

	Marcellus shale	Barnett shale	Haynesville shale	New-Albany shale
V_L (scf/ton)	200	96	60	104
T_L (psi)	500	650	1500	412
Bulk density (gr/cc)	2.46	2.58	2.6	2.4
Critical pressure (psi)	3000	1500	2000	2000
Porosity	0.06	0.06	0.08	0.06
Permeability (md)	0.00005	0.00001	0.00001	0.00001
Initial pressure (psi)	5000	4000	9000	6000
Compressibility (psi^{-1})	0.000003	0.000003	0.000001	0.000001
Temperature (F)	220	180	300	90

$$\frac{d\phi}{dp} = 0 \tag{2}$$

3. Porosity and permeability change in shale

The changes in porosity and permeability of shale matrix occur when production starts. This variation in porosity and consequently permeability is because of two reasons; gas desorption from shale surface (unlike conventional reservoirs) and increasing effective stresses by pressure depletion. When gas molecules leave the surface of the shale rock and move toward the pore spaces, in fact the pore volume is increased as the matrix volume is decreased. This will result in an increase in porosity of the shale matrix. Unlike desorption effect, the porosity of shale tend to decrease with production as a result of increased net stress effect. The change in porosity and subsequent permeability of the shale has not been studied in the reservoir simulation while focusing on its effect on a long-term production outlook. Therefore, the mathematical background of the porosity and permeability changes in shale matrix is presented herein.

Generally, in early stages of production from shale formations as the reservoir pressure is considerably high, there is no significant desorption from shale surface to contribute to production. This means that up to some stages of production, reservoir is encountered with porosity reduction due to increased net stress and compaction. Once a critical life time of a shale reservoir is reached, the porosity change due to desorption must be considered in which porosity will enhance due to increase of pore volume of shale and consequent reduction in rock volume. This critical life time of a shale reservoir depends on its isothermal desorption behavior that should be measured experimentally. After the critical period of shale production is passed, three different scenarios are possible. First, the compaction effect on porosity dominates the porosity change against desorption and the total effect tend to reduce shale porosity. Second, the two effects may not overcome each other that means the porosity reduction due to compaction is balanced by its enhancement due to desorption. Last, porosity increases several orders of magnitude more than its reduction due to compaction. These three scenarios are all observed among results of this study.

For the formulation of our first objective, the procedure and mathematical background is provided in the following. The porosity is expressed as a function of pore volume (PV) and the bulk volume (BV) as given in Eq. (3), and then expanded over pressure by Eq. (4).

$$\phi = f(V_P, V_B) \tag{3}$$

and

$$\frac{d\phi}{dp} = \left(\frac{\partial\phi}{\partial V_P}\frac{dV_P}{dP}\right)_{V_B}\left(\frac{\partial\phi}{\partial V_B}\frac{dV_B}{dP}\right)_{V_P} \tag{4}$$

Bulk volume can be represented as a function of pore and rock volumes and by manipulation we get Eq. (5).

$$\frac{d\phi}{dp} = C_R\phi + \left(\frac{\partial\phi}{\partial V_R}\frac{dV_R}{dP}\right)_{V_P} \tag{5}$$

Also, the equality of $(dV_R/dp) = (dV_{ads.}^{rock}/dp)$ holds, since the volume of grains are constant.

Further, since the adsorbed gas volume measurement is difficult, we need to relate the volume of the released gas to the adsorbed gas volume through the mass balance of the desorbed gas given by Eq. (6).

$$\rho_g^{ads.}V_{ads.}^{rock} = \rho_g^{free}V_{ads.} \tag{6}$$

where ρ_g^{ads} and $V_{ads.}$ are the density of adsorbed gas and the released gas volume, respectively. ρ_g^{free} represents the density of free gas that is further defined Eq. (7).

$$\rho_g^{free} = \frac{PM}{ZRT} \tag{7}$$

where M, Z, R, T are the gas molecular weight, compressibility factor, gas constant, and temperature, respectively. Released gas volume at any pressure defined as:

$$V_{ads.} = \frac{V_L P}{P_L + P}B_g \tag{8}$$

and

$$B_g = 0.0283\frac{ZT}{P} \tag{9}$$

when plug these back into Eq. (6), we get Eq. (10).

$$V_{ads.}^{rock} = \frac{\rho_g^{free}}{\rho_g^{ads.}}\left(B_g\frac{V_L P}{P_L + P}\right) = \frac{0.0283M}{\rho_g^{ads.}R}\left(\frac{V_L P}{P_L + P}\right) \tag{10}$$

Incorporating Eqs. (8)–(10) with Eq. (4), Eq. (11) is obtained:

$$\frac{d\phi}{dp} = C_R\phi - \left(\frac{0.0283MV_L P_L}{\rho_g^{ads.}R}\left[\frac{\phi^2}{V_P(P_L + P)^2}\right]\right) \tag{11}$$

In order to use Eq. (11) to determine and plot the porosity changes, first we need to calculate V_P because it varies slightly during each time step due to desorption and rock compaction. With a simple integration of Eqs. (6) and (10), we get Eq. (12).

$$V_R = V_R^o, \quad P \geq P_{crit} \tag{12}$$

$$V_R = V_R^o - \frac{0.0283MV_L P_L}{\rho_g^{ads.}R(P_L + P)}, \quad P < P_{crit} \tag{13}$$

$$V_P = \frac{\phi}{1-\phi} V_R \tag{14}$$

and for the permeability, we used simple empirical formula introduced by Ref. [15] that is expressed in Eq. (15).

$$k = k_i \left(\frac{\phi}{\phi_i}\right)^n, \quad 3 < n < 10 \tag{15}$$

Now, proper equations are derived that suffice determination of desorption-induced porosity and permeability changes for shale. By numerical integration of Eq. (11) and incorporating Eqs. (12)–(15), the porosity change versus reservoir pressure is calculated and plotted versus pressure in the subsequent sections.

For the permeability, from a petrophysical point of view, there is no true relationship between porosity and permeability, specifically for shale rock. However, permeability is proportional to the squared of a characteristic length of the system. Hence, considering the same trend and using an empirical expression for variation of permeability dependency on porosity will satisfy our quest for calculating such data, and will not add very much error if the permeability ranges in an acceptable bound. Another assumption is homogenous and isotropic through the entire field. This might not seem realistic but is a common practice in reservoir engineering studies, as the results will provide invaluable insights.

For the Marcellus shale, the plot of porosity and permeability changes versus the pressure is given in Fig. 2. At the beginning of production, reservoir pressure is 7500 psi and by pressure depletion of the reservoir as a result of production, the porosity is decreased and consequently the permeability does until reservoir pressure reached its critical pressure around 3000 psi. A sharp increase in porosity due to desorption after the critical pressure is observed that is in agreement with the high capability of Marcellus shale in releasing gas from its nano-pores that is shown in Fig. 1. The permeability has the same trend, but sharper decline.

In the case for Barnett and New Albany shales, Figs. 3 and 4, similar trend is observed but with smoother decrease and increase for porosity and ultimately the permeability. This result demonstrates less capability of these formations in releasing the

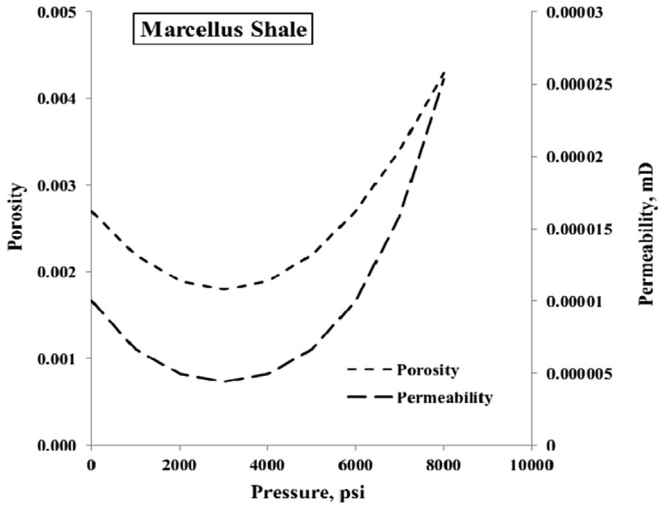

Fig. 2. Marcellus shale porosity/permeability change.

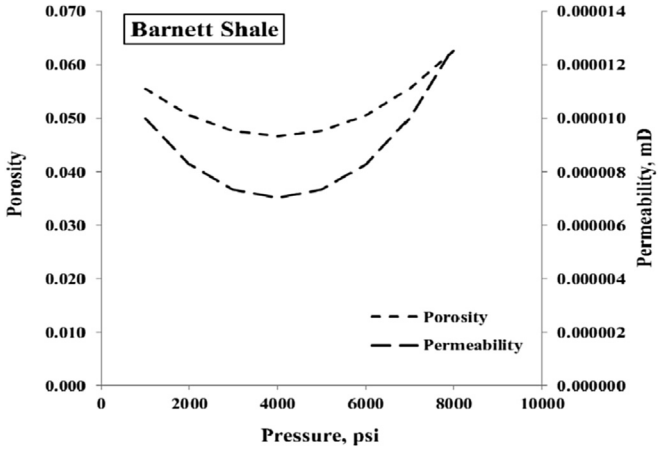

Fig. 3. Barnett shale porosity/permeability change.

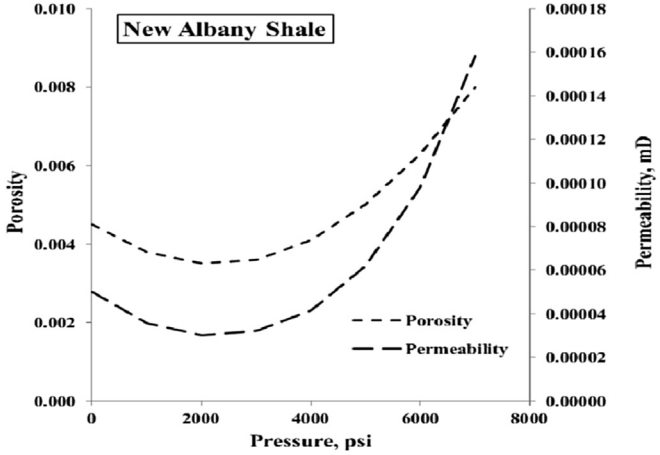

Fig. 4. New Albany shale porosity/permeability change.

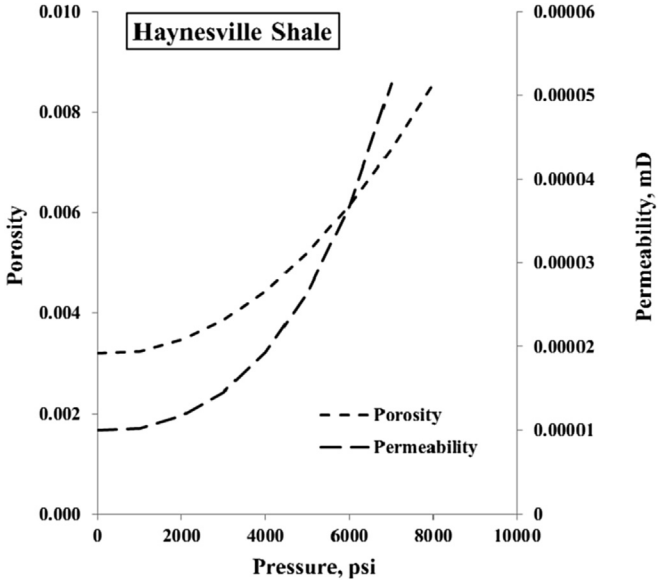

Fig. 5. Haynesville shale porosity/permeability change.

gas and subsequently providing more pore volume in the bulk of porous rock.

The slope of porosity change versus pressure is observed to be positive along the pressure depletion of the Haynesville shale (Fig. 5). This is mainly associated to the small amount of Haynesville rock desorption of methane. This is in an agreement with the experimentally measured isothermal desorption curves given in Fig. 1. The change in permeability is sharper, but has followed the same trend.

4. Closures of hydraulic fractures

The permeability (or conductivity) of both hydraulic and natural fractures are easily influenced by changes of stress and strain during gas production from shale. Therefore, incorporating pressure dependency of fractures permeability in reservoir modeling and simulation process is a significant step towards more realistic assessments of production behavior of shale reservoirs.

The geomechanical properties of Marcellus shale is investigated by Ref. [16]. They generated rock mechanical properties, geomechanical well logs, and studied various characteristics such as minimum horizontal stress, Young, bulk shear modulus, as well as Poisson's ratio that play an important role in defining the stress profiles of an unconventional reservoir. Moreover, having an access to rock's geo-mechanical properties enhances the understanding of parameters, such as conductivity and pressure dependency of permeability [17].

Research studies and experiments are conducted to analyze hydraulic fracture sensitivity to the change of effective stress profile of the reservoir by continued production [18]. Eq. (16) presents pressure dependency of permeability that is derived from experimental studies published by Refs. [19,20] that generated a conductivity multiplier chart based on their experimental data in order to implement in a commercial reservoir simulation. We used this table to express the relationship between permeability and pore pressure change with an exponential mathematical expression given in Eq. (16).

$$k = k_{\mathrm{hi}} e^{-d_{\mathrm{h}}\Delta p} \tag{16}$$

where k is hydraulic fracture permeability (the block that hydraulic fracture is located), k_{hi} is initial hydraulic fracture permeability, d_{h} is exponential decay constant determined by experiments and $\Delta p(p - p_{\mathrm{initial}})$ is average reservoir pressure minus initial reservoir pressure in psi. The exponential decay constant is calculated by curve fitting or even by handling a history match process for each specific shale [6]. The acceptable values are provided in Eq. (17).

$$10^{-3}\left(\frac{1}{\mathrm{psi}}\right) < d_{\mathrm{h}} < 10^{-6}\left(\frac{1}{\mathrm{psi}}\right) \tag{17}$$

5. Description of gas flow model

In order to compare the results of the effect of desorption-induced porosity and permeability of all four shales on natural gas production, a same horizontal well is drilled into all four formations. A horizontal well with 14 hydraulic fracture stages spaced uniformly along its entire length. The common fracture height is $h_{\mathrm{f}} = 200$ ft, and the tip-to-tip length of each fracture is $2l = 700$ ft perpendicular to h_f. The distance between the hydraulic fractures is $2d = 300$ ft. Gas flows into each fracture plane from both sides, and the permeability of hydraulic fractures is assumed to relate to average reservoir pressure through an exponential function given by Eq. (16), but its initial effective permeability is higher than the rock matrix and natural fractures feeding gas into it. Total amount of 28 pieces (twice as the number of hydraulic fractures) of simple model shown in Fig. 6 is combined to calculate the total production of the horizontal well.

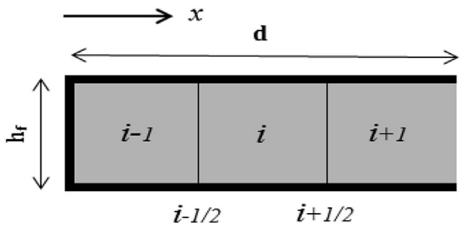

Fig. 6. Simple shale model.

In this study, Darcy's law handles gas flow through a complex system of fractures, cracks and re-opened natural fractures. This multi-scale and complexly connected flow system is treated at the end by hydraulic fractures of shale rock that is given by right hand-side of Fig. 6. Stored gas inside pores as well as adsorbed gas on rock surface fed to main hydraulic fracture planes through flow along paths that are perpendicular to the hydraulic fractures that is treated as linear flow. During the production, pressure in the tubing that is fed by hydraulic fractures is kept at 500 psi in all four shale cases, again, for the sake of comparison.

5.1. Governing equations

The general mass balance expression for a one dimensional single phase gas flow in porous rock is given by Eq. (18).

$$-\frac{\partial(\rho_{\mathrm{g}} u_{\mathrm{g}})}{\partial x} = \frac{\partial\left[\phi\rho_{\mathrm{g}} + (1-\phi)\rho_{\mathrm{gsc}}\rho_{\mathrm{b}} G\right]}{\partial t} \tag{18}$$

where u_{g} is the velocity of gas defined by Darcy law, ρ_{g} is free gas density; ρ_{gsc} is the gas density in standard atmospheric condition, G is potential releasable-gas content in scf/t in Langmuir model, ρ_{b} is shale matrix density and ϕ is rock porosity. In this study, as it is mentioned previously, unlike most reservoir simulation and modeling procedures, the porosity is not kept constant throughout the production life of the reservoir. Darcy's law and Langmuir isotherm model is applied to the linear, horizontal flow of gas as given by Eqs. (1) and (19), respectively.

$$u_{\mathrm{g}} = \frac{k}{\mu}\frac{\partial p}{\partial x} \tag{19}$$

One important assumption in this section is as follows. Due to very low porosity of shale rock we can accurately assume: $(1 - \phi) = 1$.

Further, we incorporated the Klinkenberg modification on gas permeability to Darcy's law given by Eq. (20).

$$k = k_{\mathrm{d}}\left(1 + \frac{b}{P}\right) \tag{20}$$

where b is in psi, the Klinkenberg slippage factor and P is the reservoir pressure.

5.2. Physical properties of gas

Shale gas reservoirs similar to other hydrocarbon reservoirs are in a very high temperature and pressure conditions. Physical behavior of natural gas is very nonlinear under such conditions and considering the ideal gas equation of state (EOS) results in an inaccurate evaluation of unconventional assets. Peng-Robinson (PR) EOS is used in this study and is incorporated and developed in the numerical scheme. A cubic equation of PR EOS is expressed by compressibility factor that is given by Eq. (21).

$$Z^3 + sZ^2 + qZ^1 + r = 0 \tag{21}$$

where $\begin{cases} s = B - 1 \\ q = A - 3B^2 - 2B \\ r = -AB + B^2 + B^3 \end{cases}$, $\begin{cases} A = aP/(R^2T^2) \\ B = bP/(RT) \end{cases}$, where A, B, a and b are dimensionless parameters that are easily calculated from critical properties of natural gas. The molar density of gas is defined as Eq. (22).

$$\rho_g = \frac{p}{RTZ} \tag{22}$$

For the viscosity of real gases, method developed by Ref. [21] is applied to the model and Eq. (23) is derived by Dempsey [22].

$$\mu = \mu_{g1} \exp\left\{ \ln\left(\frac{\mu_g}{\mu_{g1}} T_{pr} \right) \right\} \Big/ T_{pr} \tag{23}$$

where
$\mu = (1.7 \times 10^{-5} - 2.1 \times 10^{-6}\gamma_g)(1.8T + 32) + 8.2 \times 10^{-3} - 6.2 \times 10^{-3} \log \gamma_g$ and also $((\mu_g/\mu_{g1})T_{pr})$ can be expressed as a function of pressure, temperature; T_{Pr} is the pseudo reduced temperature of the gas and γ_g is the relative density.

5.3. Finite difference approximations

The finite differential equation describing the mass conservation can be spatially and temporally discretized to obtain the non-linear algebraic equation given by equation below.

For temporal derivative backward difference is used expresses as in Eq. (24).

$$\frac{\partial(\phi\rho_g)}{\partial t} + \frac{\partial(\rho_{gsc}\rho_b G)}{\partial t} = -\frac{\left[(\phi\rho_g) + \left(\rho_{gsc}\rho_b \frac{V_L P}{P+P_L}\right)\right]_i^{n+1}}{\Delta t} - \frac{\left[(\phi\rho_g) + \left(\rho_{gsc}\rho_b \frac{V_L P}{P+P_L}\right)\right]_i^{n}}{\Delta t} \tag{24}$$

The spatial derivatives are discretized with central difference approximation with a step size of $\Delta x/2$ as follows in Eq. (25).

$$\frac{\partial}{\partial x}\left[\rho_g \frac{k_d}{\mu}\left(1 + \frac{b}{P}\right)\frac{\partial P}{\partial x}\right] = \frac{1}{\Delta x_i}\left(\left[\rho_g \frac{k_d}{\mu}\left(1 + \frac{b}{P}\right)\right]_{i+1/2}^{n+1} \frac{P_{i+1}^{n+1} - P_i^{n+1}}{\Delta x_{i+1/2}} - \left[\rho_g \frac{k_d}{\mu}\left(1 + \frac{b}{P}\right)\right]_{i-1/2}^{n+1} \frac{P_i^{n+1} - P_{i-1}^{n+1}}{\Delta x_{i-1/2}}\right) \tag{25}$$

for $i = 1,2,3\ldots,N_{Block}$ where in above: superscript n indicates the time level, and i is the grid block index and N_{Block} is the number of grid blocks. This equation is written for all of the grid blocks; therefore there are N_{Block} independent equations. The unknown in each grid block are pressure. The value of the parameters that need to be evaluated at the spatial location of $j \pm 1/2$ refers to the values at the boundary of the adjacent grid blocks, and, as it is a common ground for reservoir simulation practice, up winding, is used to calculate their values. Once the pressures are calculated, then for the next step porosity and permeability values are updated from an equation fitted to Figs. 2–5 before starting the next time step.

5.3.1. Initial and boundary conditions

Initial condition of the system is the initial reservoir pressure given by Eq. (26).

$$P(x, t = 0) = P_{initial} \tag{26}$$

and the first boundary condition is at the left hand side (grid block #1) of Fig. 6 that has no flow (or we can say that pressure at the middle distance between two fractures has the maximum pressure) given in Eq. (27).

$$\partial p/\partial x = 0 \quad \text{at } x = 0 \tag{27}$$

The other boundary condition (the boundary at the right hand side of Fig. 1) is the specified pressure at the outlet given by Eq. (28).

$$P = \text{BHP(bottom hole pressure)} \quad \text{at } x = d \tag{28}$$

5.3.2. Solution method

We used a fully implicit approach because of the nonlinearity of the governing equation to solve Eq. (18) as this assures the most credible results with minimal errors and instabilities. Further, the Newton–Raphson method is used as our nonlinear iterative solution method. The general scheme is given by Eq. (29).

$$x^{n+1} - x^n = j^{-1} f \tag{29}$$

In brief, where x^{n+1} is the unknown vector at time $n + 1$ or next time step, x^n is the vector of unknowns in the previous time step, J is the matrix of derivatives (for the sake of speed, we used analytical derivatives instead of numerically handling the derivatives) of the residual equations with respect to the unknowns, and f is the residuals vector. At the end of each time step, the calculated material balance error, that is a sign of convergence, is negligible.

6. Results and discussions

The main outcomes of this study are first, quantifying the porosity and permeability changes of shale's gas resources due to desorption. We successfully demonstrated this in previous sections, and second, a systematic evaluation on the effect of desorption-induced porosity, permeability and geomechanics on long-term production behavior of shale reservoirs that is explained here after solving the gas flow in the simple shale model and calculating the cumulative natural gas production of each case for long-term, 25 years.

The very first observed impression is related to the fact that all of four shales are affected by the porosity and permeability changes along with geomechanics caused from methane desorption, as shown in Figs. 2–5. It is not a surprise that all of these assets are affected; however, the significant observation is that all of the four rocks are overestimated in regards to production and single well future performance evaluation if constant properties were assumed. Although it was seen that the porosity and consequently permeability are increased after the

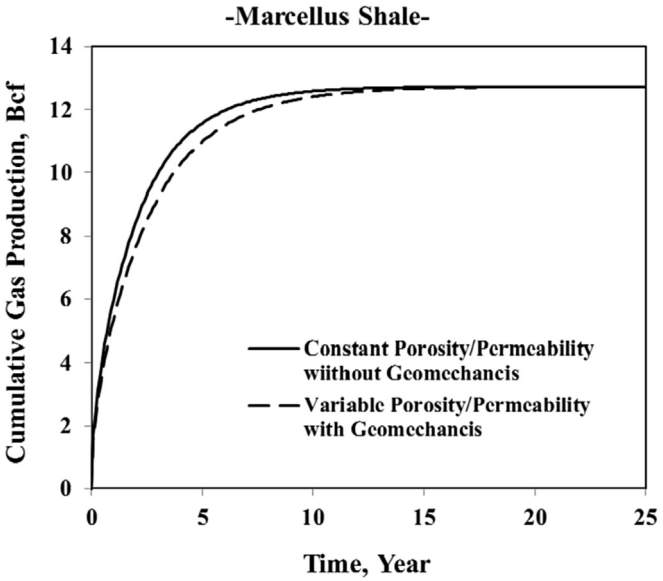

Fig. 7. Cum. gas production of Marcellus shale.

critical pressure is reached, the production outlook of 25 years is always slower, and we believe the reason is associated to the hydraulic fracture closure effect that is taking control over production with a stronger power. This in turn shows that the main flow path, hydraulic fractures, controls the production in shale reservoirs.

Fig. 7 shows 25 years of production from a horizontal well drilled in depth of 8000 ft in Marcellus shale. This well is almost has drained its stimulated reservoir volume after 10 years. Slower rate of production is observed considering changes in porosity/permeability and geomechanics that has elongated the production life of the well, that off course reached the same maximum value as the Original Gas In Place (OGIP) is constant. The effect of those changes is not huge as although the changes in porosity and permeability with reservoir pressure were observed in a sharp trend.

Figs. 8 and 9 are cumulative production during 25 years of Barnett and New Albany shales, respectively. First impression is

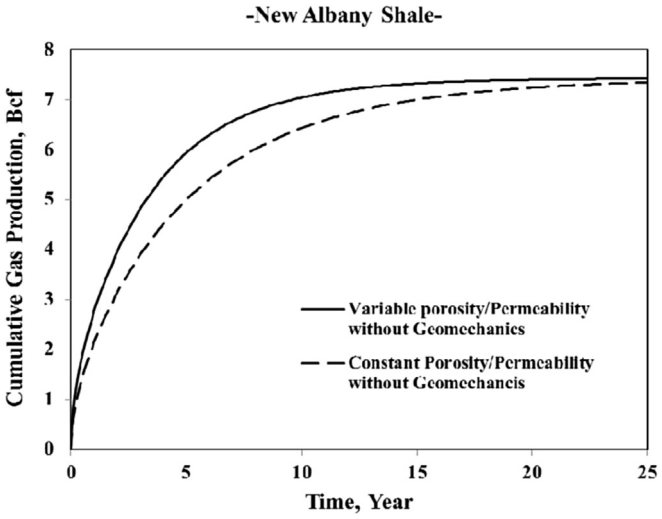

Fig. 9. Cum. gas production of New Albany shale.

that both of these shales are affected with a same scale. This is mainly because of the similarity in their desorption isotherms. It is important to notice that the New Albany shale has an effect through the production period of 25 years shown in Fig. 9. We support this with the fact that hydraulic fracture's closure is significant and are not similar to other cases after 10–15 years.

Finally, 25 years of gas production of Haynesville is shown in Fig. 10. Due to very small amount of desorption from Haynesville shale according to its experimentally measured isotherms, the effect of porosity/permeability change on production is minimum, however, the effect of geomechanics is obviously captured. This, again, demonstrates that closure of hydraulic fractures will mainly control long term production from shales. This is also in an agreement with an analytical approach that authors have published recently [20,21].

7. Conclusions

The concluding remarks of this paper are itemized below.

i) Using the laboratory measured desorption isotherms and the mathematically driven changes in porosity and

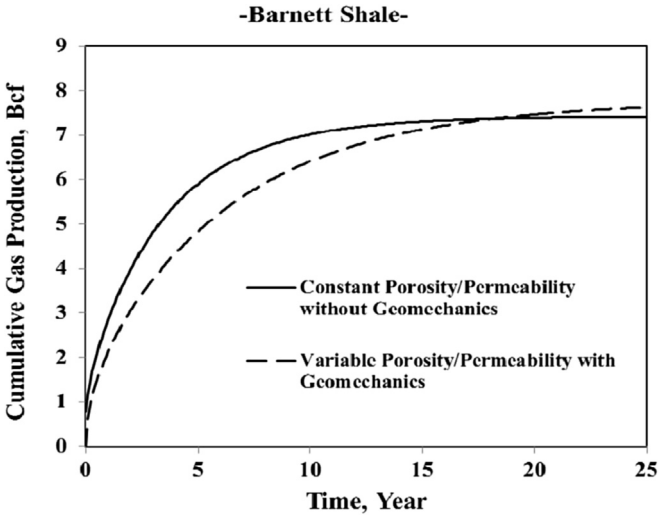

Fig. 8. Cum. gas production of Barnett shale.

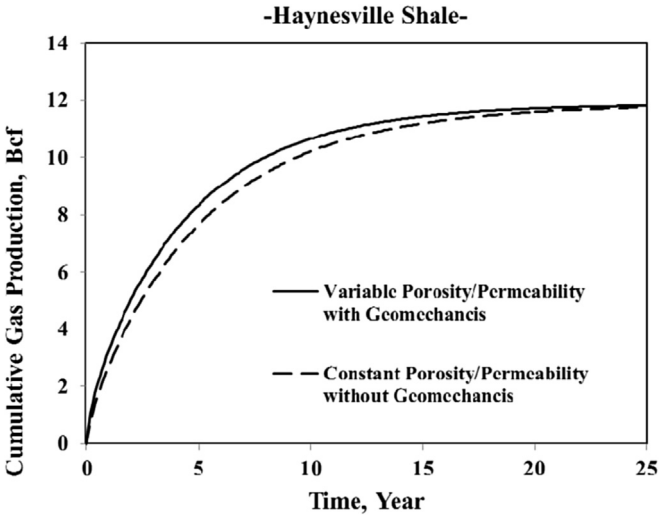

Fig. 10. Cum. gas production of Haynesville shale.

permeability of shale, we plotted such changes for the entire production life of four U.S. major shale assets that provides invaluable insights into studying such resources.

ii) It is demonstrated that the cumulative gas production from a single horizontal well is highly affected to the changes in porosity and permeability induced by methane desorption from shale rock that has been ignored in other shale gas modeling studies.

iii) It is found that larger the desorption capability of the formation (i.e. Marcellus), more severe the effect of porosity and permeability changes would be. The opposite is also confirmed for less capable rock (i.e. Haynesville).

iv) Over estimation of production from the horizontal shale wells is observed in all four assets if the desorption induced effects are not taken into account.

v) The effect of hydraulic fracture closure on production forecast is also observed in all cases, and in some assets this effect much more is stronger than the others. Marcellus shale could roughly defeat this closure effect.

vi) Furthermore, the natural gas plays a critical role to U.S. economy during this shale boom as well as by expert's projection of shale in supporting energy for next decades; hence, even small corrections to the evaluation of such formations in regards to production and their more accurate forecast is off practical interest and significance for oil & gas industry.

In our next paper, we will present the application of our model to real-field production data, incorporating non-Darcy flow and also using BET multi-layer desorption isotherm instead of Langmuir.

References

[1] V. Kuuskraa, S. Stevens, T. Van Leeuwen, et al., World Shale Resources: An Initial Assessment of 14 Regions Outside the United States, Report prepared for US Energy information Administration, Office of Energy Analysis, U.S. Department of Energy, 2011.

[2] C.L. Cipolla, E.P. Lolon, J.C. Erdle, B. Rubin, Reservoir modeling in shale-gas reservoirs, SPE Reserv. Eval. Eng. 13 (4) (2010) 638–653. SPE 125530-PA.

[3] F. Javadpour, D. Fisher, M. Unsworth, Nanoscale gas flow in shale gas sediments, J. Can. Pet. Technol. 46 (10) (2007). PETSOC-07-10-06.

[4] Y. Cho, E. Ozkan, O.G. Apaydin, Pressure-dependent natural-fracture permeability in shale and its effect on shale-gas well production, SPE Reserv. Eval. Eng. 16 (02) (2013) 216–228.

[5] M.L. Brown, Analytical Trilinear Pressure Transient Model for Multiply Fractured Horizontal Wells in Tight Shale Reservors, M.Sc. Thesis, Colorado School of Mines, Golden, Colorado, 2009.

[6] M.O. Eshkalak, U. Aybar, K. Sepehrnoori, An integrated reservoir model for unconventional resources, coupling pressure dependent phenomena, Paper SPE 171008 presented at the 2014 SPE Eastern Regional Meeting Held in Charleston, West Virginia, USA, 21–23 October, 2014.

[7] Mohammad O. Eshkalak, Shahab D. Mohaghegh, Soodabeh Esmaili, Geomechanical properties of unconventional shale reservoirs, J. Pet. Eng. 2014 (2014), http://dx.doi.org/10.1155/2014/961641. Article ID 961641, 10 pages.

[8] R.G. Moghanloo, F. Javadpour, Applying method of characteristics to determine pressure Distribution in 1D shale-gas samples, SPE J. 19 (03) (2014) 361–372, http://dx.doi.org/10.2118/168218-PA.

[9] U. Aybar, M.O. Eshkalak, K. Sepehrnoori, T.W. Patzek, The effect of natural fracture's closure on long-term gas production from unconventional resources, J. Nat. Gas Sci. Eng. 21 (2014) 1205–1213, http://dx.doi.org/10.1016/j.jngse.2014.09.030.

[10] U. Aybar, W. Yu, M.O. Eshkalak, K. Sepehrnoori, T. Patzek, Evaluation of production losses from unconventional shale reservoirs, J. Nat. Gas Sci. Eng. 23 (2015) 509–516, http://dx.doi.org/10.1016/j.jngse.2015.02.030.

[11] M.O. Eshkalak, E.W. Al-Shalabi, A. Sanaei, U. Aybar, K. Sepehrnoori, Simulation study on the CO_2-driven enhanced gas recovery with sequestration versus the re-fracturing treatment of horizontal wells in the US unconventional shale reservoirs, J. Nat. Gas Sci. Eng. 21 (2014) 1015–1024, http://dx.doi.org/10.1016/j.jngse.2014.10.013.

[12] S.A. Mengal, R.A. Wattenbarger, Accounting for adsorbed gas in shale gas reservoirs, Paper SPE 141085 presented at the SPE Middle East Oil and Gas Show and Conference, Manama, Bahrain, 25–28 September, 2011.

[13] I. Langmuir, The adsorption of gases on plane surfaces of glass, mica and platinum, J. Am. Chem. Soc. 40 (1918) 1403–1461.

[14] A. Leahy-Dios, M. Das, A. Agarwal, R.D. Kaminsky, Modeling of transport phenomena and multicomponent sorption for shale gas and coalbed methane in an unstructured grid simulator, Paper SPE 147352, SPE Annual Technical Conference and Exhibition, Denver, CO, October 30–November 2, 2011.

[15] R. Raghavan, L.Y. Chin, Productivity changes in reservoirs with stress-dependent permeability, Paper SPE 88870 Presented at the SPE ATCE, San Antonio, Texas, USA, 29 September–2 October, 2004.

[16] M.O. Eshkalak, S.D. Mohaghegh, S. Esmaili, Synthetic, geomechanical logs for Marcellus shale, Paper SPE 163690 Presented at 2013 Digital Energy Conference and Exhibition held in the Woodlands, Texas, USA, 5–7 March, 2013.

[17] M. Omidvar Eshkalak, Synthetic Geomechanical Logs and Distributions for Marcellus shale, MSc. Thesis, West Virginia University, Morgantown, West Virginia, 2013.

[18] Q. Tao, A. Ghassemi, C.A. Ehlig-Economides, Pressure transient behavior for stress-dependent fracture permeability in naturally fractured reservoirs, in: Paper SPE 131666 Presented at the CPS/SPE International Oil and Gas Conference and Exhibition, Beijing, China, 8–10 June, 2010.

[19] U. Aybar, Investigation of Analytical Models Incorporating Geomechanical Effects on Production Performance of Hydraulically and Naturally Fractured Unconventional Reservoirs, MSc Thesis, The University of Texas at Austin, Austin, Texas, 2014.

[20] U. Aybar, M.O. Eshkalak, K. Sepehrnoori, T.W. Patzek, Long term effect of natural fractures closure on gas production from unconventional reservoirs, Paper SPE 171010 Presented at the 2014 SPE Eastern Regional Meeting, held in Charleston, West Virginia, USA, 21–23 October, Society of Petroleum Engineers, 2014.

[21] Mohammad O. Eshkalak, Umut Aybar, Kamy Sepehrnoori, On the feasibility of re-stimulation of shale wells, Pet. Sci. 12 (3) (2015) 553–559.

[22] J.R. Dempsey, Computer routine treats gas viscosity as a variable, Oil Gas J. 63 (1965) 141–143.